JOURNAL OF AIRCRAFT
Vol. 46, No. 3, May–June 2009

Structural Analysis and Testing of an Ultralight Unmanned-Aerial-Vehicle Carbon-Composite Wing

R. Warsi Sullivan*
Mississippi State University, Mississippi State, Mississippi 39762
Y. Hwang†
Spirit AeroSystems, Wichita, Kansas 67278
and
M. Rais-Rohani‡ and T. Lacy§
Mississippi State University, Mississippi State, Mississippi 39762

DOI: 10.2514/1.36415

This paper presents the results of an investigation examining the strength and stiffness characteristics of a carbon composite wing of an ultralight unmanned aerial vehicle. The wing consists of foam-core sandwich skins and multiple spars with varying laminate ply patterns and wall thickness dimensions. A three-tier whiffletree system is designed and used to load the wing in a manner consistent with a pull-up-maneuver condition. Multiple strain and deflection gauges are used to measure the static response of the wing at several spanwise and chordwise locations, and the wing is loaded incrementally beyond the limit and design ultimate loads to the point of structural failure. A geometric nonlinear finite element model is developed that accounts for the variations in laminate geometry of each component as well as the properties of the adhesively bonded joints in the wing assembly. By carefully matching the boundary conditions with those of the experimental setup, the static response of the wing under a simulated whiffletree loading condition is obtained. The strain and deflection predictions from the finite element simulations are found to be in good agreement with the experimental observations. Despite its light weight, the wing is found to be very strong, with a strength-to-weight ratio of more than 40 at failure.

I. Introduction

IN RECENT years, there has been a rapid growth in design and development of different classes of unmanned aerial vehicles (UAVs) ranging from the short-range remotely piloted micro aerial vehicles [1] to the large jet-powered and autonomous UAVs. Primary uses of UAVs are usually related to the defense industry to improve U.S. surveillance and communication capabilities for homeland security operations, but UAVs are also finding increased employment in civilian airspace for monitoring coastal waters, aiding fire-fighting efforts, or gathering other valuable data [2] in an economical and safe manner. The UAV of interest in this study was developed from an off-the-shelf all-composite sailplane and is part of a larger effort to develop an all-composite ultralight UAV (UUAV) sensor platform using carbon-fiber-reinforced polymer composite materials and advanced sailplane technologies. With an empty weight of approximately 155 lb, this UAV falls under the ultralight aircraft category.

Figure 1 shows a CAD model of the UUAV design, inspired by high-performance sailplanes, which can accommodate an autonomous flight control system, generic sensor package, and a retractable propulsion system. The manufacturer achieves a reduction in part count and a low-cost fabrication process that does not require the use of an expensive autoclave. The UUAV structural components are designed using Federal Aviation Regulation (FAR) Part 23 (normal category) airworthiness standards. To determine the strength and stiffness characteristics of the wing and fuselage structural assemblies, a series of structural tests is performed.

This paper focuses on the static structural testing and finite element (FE) analysis of the wing structure with the load distribution and intensity in a manner consistent with a pull-up-maneuver condition. In subsequent sections of the paper, the wing geometry and structural layout, the material system, and the static loading condition are described. Moreover, the details of FE modeling and simulation and experimental testing are discussed, and strain-gauge, deflection-gauge, and load-cell data are presented.

II. Description of Wing Structure

The wing has a length (semispan S) of 217 in., root chord dimension of 29 in., and maximum airfoil thickness of 4 in. at the root section. Shown in Fig. 2, the FE idealization of the wing primary structure includes a root rib, upper and lower sandwich skins, and three (fore, main, and aft) spars with channel cross sections located at 15, 40, and 70% chord, respectively. The center, or main, spar extends inside the fuselage to form the carry-through structure (stub spar), providing the wing bending rigidity, with the shear load transfer supported by a pair of steel lift pins on each side that form the root-rib/fuselage interconnection, as shown in Fig. 3; the X and Y coordinates in Fig. 3 define the aft and outboard directions, respectively. The main spar has a tapered rectangular cross section in the carry-through region, as shown in Fig. 4. Outboard of the root rib, the fore and main spars are straight, but the aft spar kinks forward to accommodate the aileron placement (see Fig. 2). In addition to the ailerons, the wings are equipped with spoilers, with the aileron cutout and the spoiler housing visible in Fig. 2; both the aileron and spoiler are removed for analysis and testing purposes.

All structural members of the wing are made of Toray carbon-fiber/epoxy woven prepreg fabric (Toray-T700G) and unidirectional prepreg fabric (Toray-T700S), with properties given in Table 1. The upper and lower wing skins are of sandwich construction with 0.125-

---

Presented as Paper 1870 at the 47th AIAA/ASME/ASCE/AHS/ASC Structures, Structural Dynamics, and Materials Conference, Newport, RI, 1–4 May 2006; received 31 December 2007; revision received 31 December 2008; accepted for publication 18 January 2009.

*Assistant Professor, Department of Aerospace Engineering, Mail Stop 9549. Member AIAA.

†Structural Analysis Engineer. Member AIAA.

‡Professor, Department of Aerospace Engineering, Mail Stop 9549. Associate Fellow AIAA.

§Associate Professor, Department of Aerospace Engineering, Mail Stop 9549. Associate Fellow AIAA.

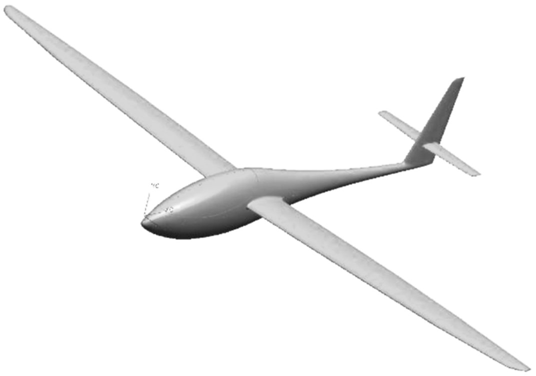

Fig. 1 CAD model of the UUAV.

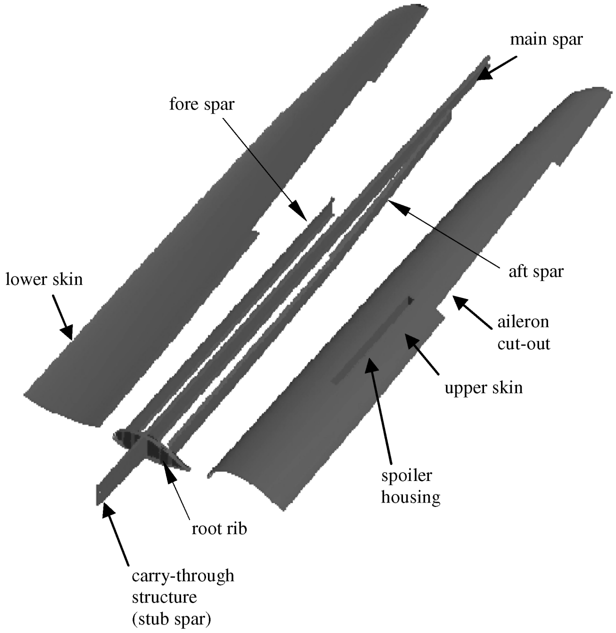

Fig. 2 Wing structural components.

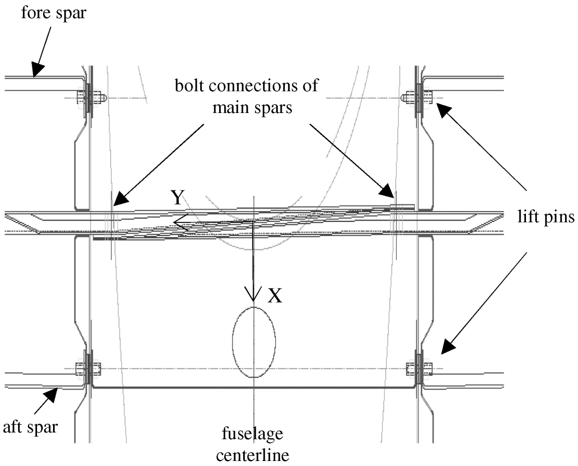

Fig. 3 Top view of the spar/spar and wing/fuselage attachment region.

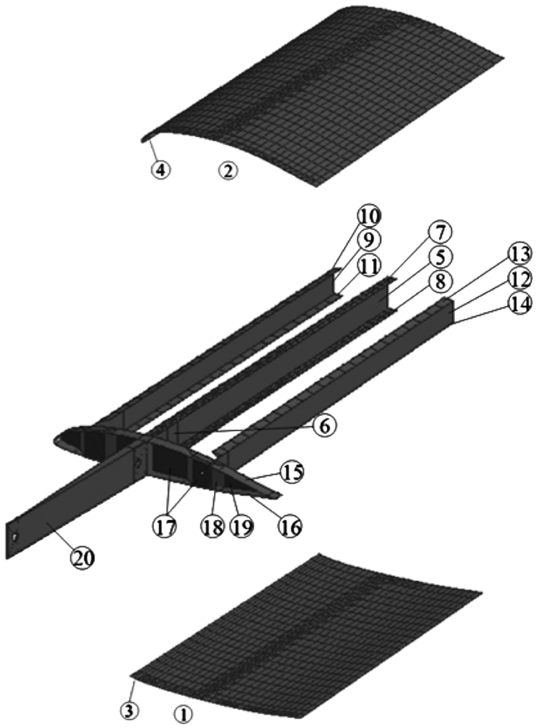

Fig. 4 Close-up view of the finite element model of structural members near the wing root, with laminate properties given in Table 2.

in-thick low-density foam core (DIAB Divinycell® HT 50). The foam core extends over the entire wing surface to about 1.5 in. from the leading edge, trailing edge, and side boundaries. The laminate ply pattern in the wing root region for individual members, identified in Fig. 4, is given in Table 2. All structural members are individually fabricated and oven-cured before being adhesively bonded in an assembly jig. The steel lift pins shown in Fig. 3 are mounted on the root rib before wing assembly.

III. Experimental Setup and Procedure

In this effort, the objective of structural testing is to measure the static stiffness and strength of the wing structure under the most critical in-flight load distribution (i.e., pull-up maneuver). Here, the load distribution is simulated using a whiffletree system, which is commonly used in the aerospace industry for the structural testing of both small and large aircraft and their components [3–5]. Depending upon the level of sophistication and intricacy of the whiffletree design, it is possible to fairly accurately simulate the distributed in-flight loads experienced by the structure. For this study, a three-tier whiffletree system is implemented. To establish the accuracy of the design, a simple finite element beam model was developed, and deflections obtained from applying concentrated loads of appropriate magnitude at four load points (as implemented by the whiffletree) were compared with deflections obtained by applying the equivalent distributed load. Because a maximum difference of only 1.2% was obtained when comparing the deflections between the two types of

Table 1 Physical and engineering properties of materials

Material property	Woven fabric Toray-T700G	Unidirectional fabric Toray-T700S	Foam-core DIAB Divinycell HT 50
E_{11}, psi	8.03×10^6	1.73×10^7	1.233×10^4
E_{22}, psi	8.03×10^6	1.35×10^6	——
G_{12}, psi	6.10×10^5	6.10×10^5	——
ν_{12}	3.00×10^{-2}	3.10×10^{-1}	3.20×10^{-1}
ρ, lb/in^3	5.40×10^{-2}	5.50×10^{-2}	1.79×10^{-3}

Table 2 Laminate definitions of structural parts in Fig. 4 at the wing root

Part no.	Description[a]	No. of plies	Ply pattern[b]
1	Bottom skin	5	$(45/0/\mathrm{foam}/0/45)_T$
2	Top skin	5	$(45/0/\mathrm{foam}/0/45)_T$
3,4	Leading edge	4	$(45/0)_s$
5	MS web	21	$(0/45)_9/45/45/45$
6	MS web root	8	$(45/0/0/45)_s$
7	MS compression cap	126	$45/45/45/[u0]_4/0/[u0]_{10}/45/[u0]_6/0/[u0]_{12}/45/[u0]_{20}/0/45/[u0]_{13}/$ $0/45/[u0]_{10}/0/45/[u0]_{10}/0/45/[u0]_{10}/0/45/[u0]_5/0/45/0/45$
8	MS tension cap	96	$45/45/45/[u0]_4/0/[u0]_6/45/[u0]_4/0/[u0]_8/45/[u0]_{14}/0/45/[u0]_6/$ $0/45/[u0]_6/0/45/[u0]_6/0/45/[u0]_{12}/0/45/[u0]_4/0/45/0/45$
9	FS web	12	$45/0/0/45/45/0/0/45/45_4$
10	FS compression cap	8	$(45/0/0/45)_s$
11	FS tension cap	8	$(45/0/0/45)_s$
12	AS web	12	$(45/0/0/45)_2/45_4$
13	AS compression cap	8	$(45/0/0/45)_s$
14	AS tension cap	8	$(45/0/0/45)_s$
15	Root-rib top	12	$(45/0/0/45/45/0)_s$
16	Root-rib bottom	12	$(45/0/0/45/45/0)_s$
17	Root-rib web	12	$(45/0/0/45)_2/45_4$
18	Root-rib AS	8	$(45/0/0/45)_s$
19	Root-rib web	4	$(45/0)_s$
20	Stub spar	8	$(45/0/0/45)_s$

[a] MS is the main spar, FS is the fore spar, and AS is the aft spar.

[b] 45 is ±45 fabric, 0 is 0/90 fabric, and $[u0]$ is unidirectional ply.

loading along the length of the beam, the whiffletree design was considered to be acceptable.

A. Loading Methodology

A universal test frame (UTF) was designed and fabricated to serve as the support structure for static strength and deflection testing (cf. Figure 5). A saddle fixture was developed for attaching the wing on the UTF in an inverted position and applying the load in the downward direction using the three-tier whiffletree system. Selected for load application and testing convenience, the downward loading of the wing requires careful consideration of the wing weight, weight distribution of the whiffletree components, and magnitude and location of the resultant force F exerted by the hydraulic load actuator. The saddle fixture, shown in Fig. 5, is designed to simulate the wing/fuselage interface geometry at the connection region (see Fig. 3). The two main spars are bolted together, and the lift pins slide into receptacles in the saddle fixture, similar to the wing/fuselage interconnection shown in Fig. 3.

The aerodynamic lift distribution on the wing was estimated using the vortex-lattice method [6] based on the wing planform geometry and airfoil data, the expected angle of attack, and the maneuver airspeed. The nearly elliptical lift distribution along the span was divided into four piecewise-linear sections, with the statically equivalent section resultant forces applied via loading cradles positioned at spanwise loading stations LS1, LS2, LS3, and LS4 at approximate distances of $0.11S$, $0.33S$, $0.55S$, and $0.77S$, respectively, measured from the fuselage centerline, as shown in Figs. 5 and 6. The ratio of the total force at each loading station to the resultant force on each wing is given in Table 3. The three tiers of the whiffletree are positioned accordingly, with the location of the load actuator closely matching that of the resultant aerodynamic force on each wing. The forces applied at each loading station for the limit load (LL) condition of 3.8-g and ultimate load (UL) condition at 5.7 g are also listed in Table 3. The components of the whiffletree system are designed to sustain a maximum resultant force of 2500 lb, which significantly exceeds the design ultimate load of each wing.

Table 3 Force distribution at wing loading stations LS1 to LS4

	LS1	LS2	LS3	LS4
Fraction of total	0.31	0.28	0.23	0.18
LL, lb	263	239	201	153
UL, lb	394	359	301	229
UL/LL	1.498	1.502	1.498	1.497

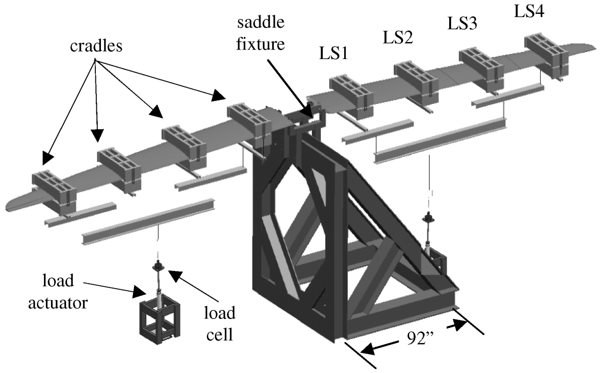

Fig. 5 Whiffletree loading system for wing static testing.

The top and bottom pieces of the wooden cradles at LS1 to LS4, shown in Fig. 5, closely match the airfoil shape at the contact surface and are bolted together to prevent slippage of the cradles while loading the wing. To distribute the loading, thereby avoiding local damage to the wing skin, the top cradles rest on a series of 1-in.-wide wooden strips (load pads) placed over and near each wing spar on both the right and left wings. The cradles are attached to the first tier of the whiffletree using steel connectors. The first- and second-tier members are aluminum channel sections, and the third tier consists of a single aluminum I-beam. The actuator/load-cell assembly, for both the right and left wings, is mounted to a surface plate on the laboratory floor via a ball bearing. This design allows rotation of the loading assembly as the wing structure deforms. A steel turnbuckle connects the I-beam to the load cell. Because the actuator's maximum stroke is insufficient to produce structural failure, the turnbuckle is used to preload the assembly to the limit load, with the actuator providing the additional load to induce failure. Each actuator is connected to a separately controlled hand pump.

B. Instrumentation

Each wing is fitted with a total of 48 strain gauges at five different wing stations, three of which are shown in Fig. 6 and identified as gauge stations (GS) 1 through 3, located at approximately $0.08S$, $0.24S$, and $0.44S$, respectively. Strain gauges are attached to all three spars (fore, main, and aft) at locations GS1 and GS3, and only the main spar has strain gauges at the GS2 location. The axial strain gauges are used to measure the normal strain at the inner surfaces of

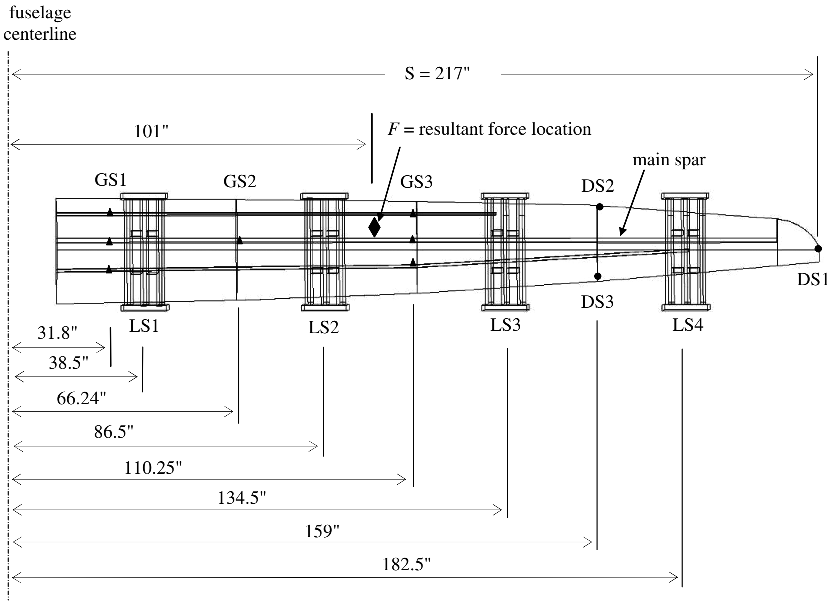

Fig. 6 Locations of loading stations, strain-gauge stations, and deflection-gauge stations.

the upper and lower spar caps, and rosette strain gauges are used to find the shear strain at the centroid in the spar web. Hence, there are six axial and three rosette strain gauges at GS1 and GS3 and two axial and one rosette at GS2. Additional strain gauges are also attached on the top and bottom caps of the right as well as the top cap of the left stub spars. The general-purpose strain gauges (Vishay Measurements CEA-06-125UR-350) have a nominal gauge length of 0.125 in. Each strain gauge was tested before bonding the upper skin to complete the wing assembly.

In addition to strain gauges, three deflection gauges (Celesco PT1DC cable-extension position transducers), with a maximum stroke length of 50 in., are used to measure the vertical deflection stations (DS) at three locations, identified as DS1, DS2, and DS3 in Fig. 6, and are also shown in Fig. 7a. DS1 is attached at the tip of the wing to obtain the maximum deflection at each load, and DS2 and DS3 are mounted at approximately $0.67S$ (between LS3 and LS4) to obtain the angle of twist.

A computer data acquisition system using LabVIEW® software [7], is used to collect load, strain, and deflection data while manually loading the structure with hand pumps. The strain gauges are zeroed with the wings resting on the laboratory floor, whereas the deflection-gauge readings are zeroed with the wing attached to the UTF under its own weight. Both load cells, as well as the deflection gauges, are calibrated before testing, and together with selected strain-gauge channels, result in a total of 80 channels being monitored simultaneously during the static testing.

Strain and deflection readings are first recorded with the wing under its own weight and then as each tier of the whiffletree is assembled. The wing structure is loaded in 100 lb increments to the limit load of 855 lb and then in 50 lb increments to failure. The applied load is the sum of the wing weight (35 lb), whiffletree weight, and the actuator force. Figure 7a shows the left wing in the testing arrangement. As seen, the first tier of the whiffletree is attached to the wooden cradles that sandwich the wing at four stations. The lead wires from the deflection gauges at DS1-DS3 are also visible, along with the actuator/load-cell assembly. Figure 7b shows the right wing at the limit load condition (855 lb) with the tip deflection δ.

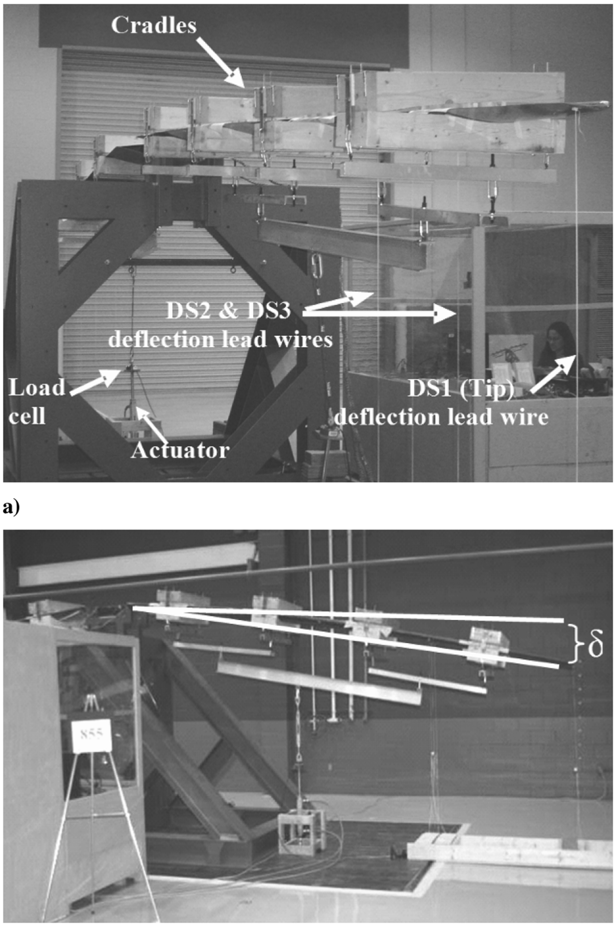

Fig. 7 Photographs of a) static test arrangement and b) wing tip deflection at limit load.

IV. Finite Element Modeling and Analysis

A. FE Model

In this study, full-scale ABAQUS [8] FE models of the UAV wing are developed to predict structural deflections and strains associated with critical loading conditions. The models account for the composite material stack-up sequence, sandwich construction, and ply dropoffs throughout the wing; a total of 281 material property regions are defined. The adhesive layer between principal structural elements (spar, root-rib/skin/spar, and skin/skin interconnections) is explicitly modeled using continuum elements to better characterize the load transfer within the structure. Because both wings are symmetric with the exception of the inboard extrusion of the main

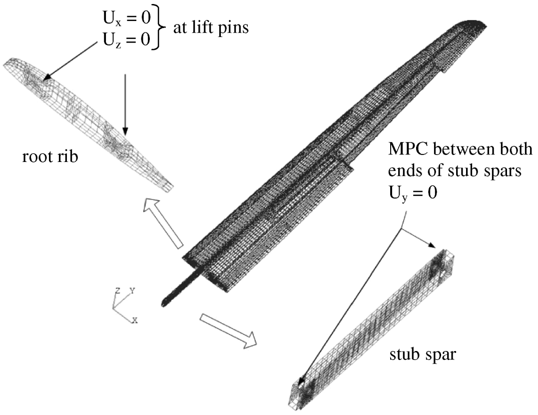

Fig. 8 Representative finite element mesh with kinematic boundary conditions for static analysis.

spar at the root (stub spars), and one wing and two stub spars are modeled using appropriate multiple-point constraints (MPCs) to simulate both wings.

Three-dimensional FE modeling and simulation of the wing primary structure involves a number of major steps. An outer mold line (OML)-geometry CAD model is used to establish a series of surfaces that are necessary to simulate the wing skins. Based on the OML surfaces, three-dimensional models of the interior principal structural elements (spars, root rib, etc.) are developed from two-dimensional CAD drawings. Essentially, this process involves specification of coordinates associated with locations of key internal cross sections, establishment of cutting planes to define the intersection of internal spar, rib, or webs with the OML, and extrusion of three-dimensional internal structures based upon two-dimensional data of cross sections at specified locations. A similar procedure is used to assign composite material properties that account for the stack-up sequence, sandwich construction, and ply dropoffs throughout the vehicle. Special care is taken to ensure that the FE mesh subdivisions coincide with ply dropoffs and other changes in materials and/or structure. Figure 8 contains a representative FE mesh for the wing, with highlighted kinematic boundary conditions at the wing root rib and stub spars. Standard anisotropic shell elements are used to simulate the composite face sheets in the skins, ribs, spar caps, spar webs, and steel cylindrical lift pins; continuum elements are used to simulate the foam-core adhesive and steel bolts defining the two stub spar interconnections. The preliminary model used in the static analysis contains 34,165 elements, 79,855 nodes, and 440,595 degrees of freedom.

B. Boundary Conditions and Loading

Kinematic boundary conditions as identified in Fig. 8 are consistent with those used in the static structural proof testing. As in Fig. 3, the X, Y, and Z coordinates in Fig. 8 define the aft, outboard, and up directions, respectively. At the simulated wing lift pin-saddle fixture interconnection, the in-plane displacements are fixed (i.e., $U_X = U_Z = 0$). Appropriate MPC equations are employed to ensure symmetry of nodal displacements and rotations at the simulated stub spar/root-rib interconnection; this effectively eliminates the need to simulate two entire wing assemblies. The simulated whiffletree loads are applied in the FE model as follows. For a prescribed value of total applied load, the load ratios in Table 3 are used to determine the resultant force at each whiffletree load station. The resultant force at each load station is applied to the lower surface of the wing as uniform normal pressures acting over the contact areas between the load pads and the skin; the magnitude of the normal pressure at each pad is selected such that the line of action of the resultant force at each station passes through the quarter-chord location for the cross section.

Table 4 Measured wing deflections and strength

Loading condition	F, lb	δ_R/S, %	δ_L/S, %	F/W
LL	855	8.87	8.67	24.4
UL	1283	13.36	13.08	36.7
Right-wing failure	1456	21.61	15.84	41.6
Left-wing failure	1550	——	17.00	44.3

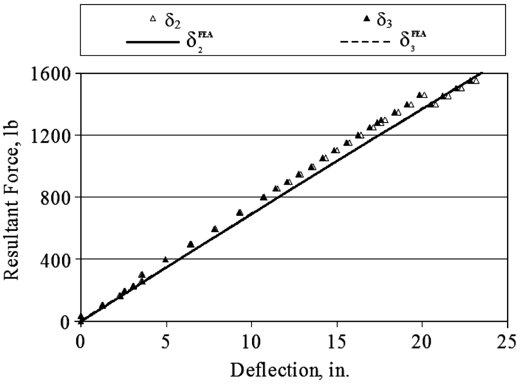

Fig. 9 Comparison of measured and predicted vertical deflection δ_2 at DS2 and δ_3 DS3 of the left wing.

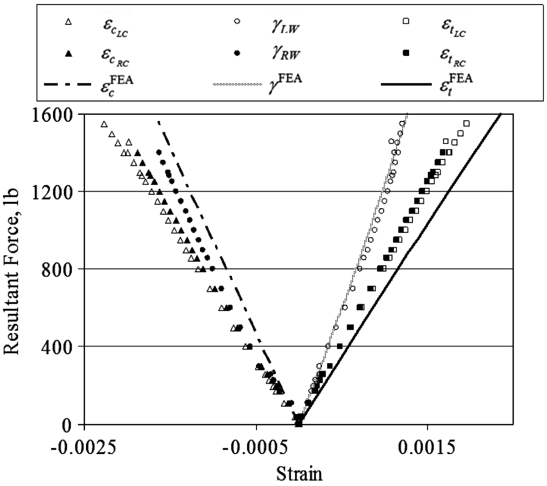

Fig. 10 Comparison of measured and predicted axial and shear strains in main spar at GS1 of the right and left wings.

C. Static Analyses

Geometric nonlinear static FE analyses are performed to predict wing deflections as well as laminate stresses and strains under incremental loading to design ultimate load. The stress and strain distributions are also used to identify the critically loaded regions of the structure as well as potential failure zones.

V. Results and Discussion

A. Experimental and Analytical Results

Table 4 lists the values for the percent relative tip deflection for the right wing (δ_R/S) and the left wing (δ_L/S), measured from the initial position of the wing tip. The ratios of applied load to wing weight (F/W) for LL, design UL, and before failure for both wings are also given. At the point of failure, the strength-to-weight ratio of greater than 40 was realized for both wings, with a right-wing tip deflection and left-wing tip deflection of 47 in. ($0.22S$) and 37 in. ($0.17S$), respectively. The point of failure corresponds to 6.4 g for the right and 6.9 g for the left wing, which are approximately 17% higher than the design ultimate load factor.

Figure 9 shows the measured and predicted deflections at stations DS2 and DS3 ($0.67S$) of the left wing as a function of applied load. At these locations, the FE predictions correlate very well with the experimentally measured values. The measured data for DS2 and DS3 of the right wing are nearly identical to those of the left wing and hence are not shown here. Also, no twist was evident, because the deflections at DS2 and DS3 are found to be almost equal for both wings.

Measured and predicted strains at GS1 ($0.08S$) and GS3 ($0.44S$) are shown in Figs. 10 and 11, respectively. The measured axial strains are from direct reading of the cap strain gauges, whereas the shear-strain values are calculated using the three normal strain measurements (at 0, 90, and 45 deg) at each web rosette. Because of the limited number of channels that could be recorded at the same time, no shear-strain measurements are taken at GS3. For ease of comparison, the strain readings taken from the right and the left wings at the same spar locations are plotted together. Axial strain at the compression cap of the left wing is identified by $\varepsilon_{c_{LC}}$ and that of the right wing is identified as $\varepsilon_{c_{RC}}$. Consistent labels are used for the spar caps in tension ($\varepsilon_{t_{\mathrm{LC}}}, \varepsilon_{t_{\mathrm{RC}}}$) and spar webs in shear ($\gamma_{\mathrm{LW}}, \gamma_{\mathrm{RW}}$).

As shown in Fig. 10, the FE estimates for the tensile and compressive main spar cap strains, as well as shear web strains, correlate reasonably well with measured values. Similar results are obtained when comparing measured and predicted strains for the fore spar tensile caps and shear web (not shown).

The FE estimates for strains at GS3 (Fig. 11) for all three spar locations correlate quite well with the measured responses; this is especially true for the aft spar location, where excellent agreement is obtained for both the tensile and compressive spar caps. The measured values indicate that the normal strains in the aft spar caps are nearly equal, but about one-half of those in the main spar caps. For both left and right wings, the normal strains in the compression caps for all three spars are almost identical, but the difference in the tensile strains in the right wing for the fore and main spars increases as the loading increases.

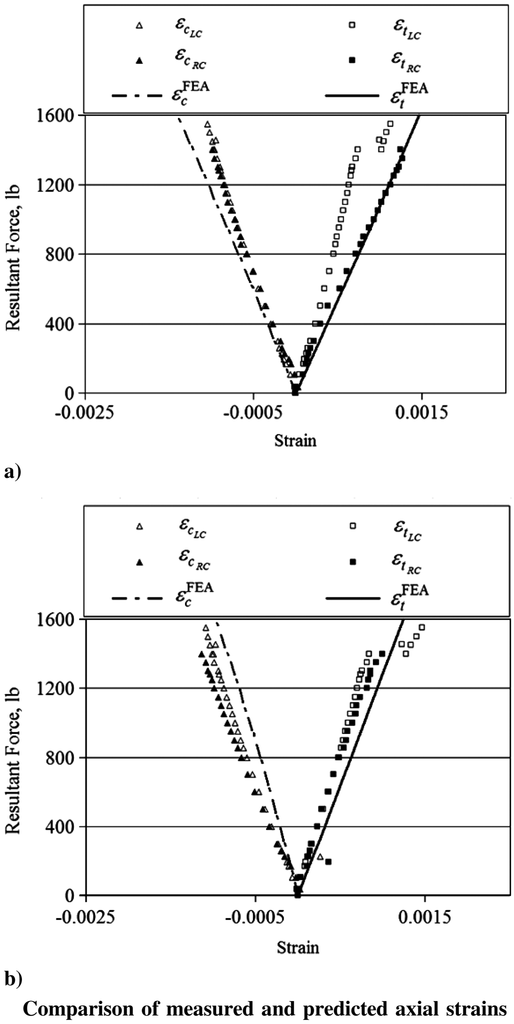

Fig. 11 Comparison of measured and predicted axial strains at GS3 (44%S) in a) fore spar and b) aft spar of the right and left wings.

As shown in Fig. 12, the primary failure location developed at the transition of the aileron cutout for both wings, also evidenced by the symmetric pattern. The right wing failed at an applied load of 1464 lb, and this was followed by failure in the left wing at 1550 lb. Both wings exceeded the design ultimate load of 1283 lb before failure. Symmetric buckling of wing skins on the right and left wings on the compressive side was observed before limit load, with relatively few acoustic emissions until close to failure. The failure occurred on the compression side of both wings and extended through all three spars. The whiffletree remained intact through the failure process.

B. Error Assessment

Possible factors that may influence the accuracy of the measured responses are explored by examining the test setup, experimental, and simulation procedures.

1. *Instrument Calibration*

Strain gauges (±3% sensitivity) in both wings were attached at the spar locations (Fig. 6) at the UUAV manufacturing site. All gauges were tested before bonding the top skin to complete the wing assembly, after which direct access to the gauges was not available. The gauge calibration procedure included zeroing all gauges with the wing assembly at the ground level. Therefore, once the wings were mounted in the test fixture, the gauge readings indicated the strains due to the wing assembly weight. Henceforth, strain data were acquired at each level of loading, and as shown in the figures, the strain data show the expected linear behavior. The deflection gauges (±0.28 to ±0.15% full stroke sensitivity) were calibrated using a five-axis precision milling machine by correlating the readings from the cable-extension gauges to the distance traversed by the milling machine in the vertical direction. The 10 kip load cell was factory-calibrated, but its accuracy was further confirmed by using precision weights and comparing the value of the weights with the readings from the load cell, which has a static error band of ±0.07%. Although some error is due to equipment (sensors and data

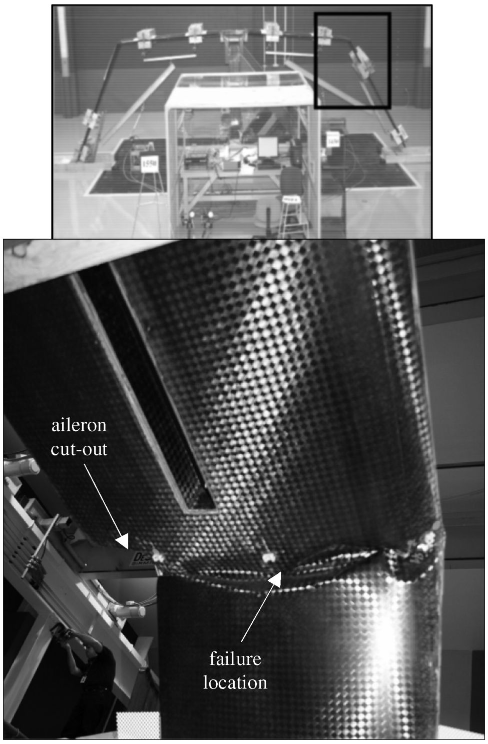

Fig. 12 Wing structure failure mode and location.

acquisition components) limitations, the resulting data show reasonable trends and magnitudes.

2. Experimental and Analysis Error Assessment

Figures 9–11 show a shift in left-wing responses after the load level of approximately 1400 lb. This shift is attributed to the initiation of failure in the left wing, as it exceeds its design ultimate load and is most visible in the tension cap data of the fore and aft spars. Below the 1400 lb load, there is fairly good consistency between the left and right wings, with the exception of the tension cap axial strains in the fore spar at GS3. The data in Fig. 10 show a sign difference between the shear strains measured in the right and left wing main spars at GS1. This difference is mainly due to the unsymmetric alignment of the rosette gauges in the two wings. Some error is also attributed to the small variations in strain-gauge locations between the right and left wings.

After failure of the wing assembly, both left and right wings were cut at multiple stations to observe both the adhesive joint and the placement of the strain gauges. This activity revealed possible reasons that may account for the difference in the experimental results when compared with the numerical predictions. Significant variations in the adhesive thickness were observed; additionally, it was noted that many strain gauges were placed in resin-rich areas and in areas of ply sequence transition. Deviations of the predictions from the experimental data are also attributed to using the vendor-supplied ply thickness and material data in the simulation. Other factors that affect the comparison with the numerical results include the loading of the wing. The simulation used kinematic boundary conditions consistent with the test and the loading was applied as a pressure load to simulate the loading of the whiffletree. However, it was observed that with increasing load, the whiffletree had a tendency to skew toward the load actuator, causing the direction of the load at each station to deviate slightly from normal to the wing surface.

Overall, the data indicate consistency in experimental measurements when observing the deflections between the right and left wings as well as most of the strain-gauge measurements. The preliminary simulation results show reasonable estimates of deflection and fairly good correlations with the measured strain.

VI. Conclusions

An overview of structural analysis and testing of a composite wing for an ultralight UAV was presented. A whiffletree system was designed and used for static loading of the wing structure with a distribution based on a pull-up maneuver. The apparatus proved effective in loading the wing structure in an incremental and controlled manner beyond the limit and design ultimate loads to the point of failure. A geometric nonlinear finite element model of the wing was also developed. The kinematic and natural boundary conditions were imposed consistently with those in the experimental setup. The load-deflection and load-strain data were collected using a computerized data acquisition system. The FE analysis predictions for the static response compared fairly well with the experimental observations and the measured data. As part of future efforts, a progressive failure analysis of the wing structure will be performed to investigate the local instability and crippling of the sandwich skin, as witnessed in structural testing.

Acknowledgment

The funding provided for this study by the U.S. Army Space and Missile Defense Command under contract DASG60-01-C-0038 is gratefully acknowledged.

References

[1] Stewart, K., Wagener, J., and Abate, G., “Design of the Air Force Research Laboratory Micro Aerial Vehicle Research Configuration,” 45th AIAA Aerospace Sciences Meeting and Exhibit, Reno, NV, AIAA Paper 2007-667, Jan. 2007.

[2] Cárdenas, E., Boschetti, P., Amerio, A., and Velasquez, C., “Design of an Unmanned Aerial Vehicle for Ecological Conservation,” Infotech@Aerospace, Arlington, VA, AIAA Paper 2005-7056, Sept. 2005.

[3] Ma, S. F., and Shiue, T. K., “Aircraft Airworthiness Certification: Static Bench Testing of an Airfoil Elevator,” *Experimental Techniques*, Vol. 27, No. 1, Jan.–Feb. 2003, pp. 32–35. doi:10.1111/j.1747-1567.2003.tb00097.x

[4] Smith, H. W., “Static Test of an Ultralight Airplane,” *Journal of Aircraft*, Vol. 25, No. 1, 1988, pp. 37–40. doi:10.2514/3.45538

[5] Wong, A., and Luke, G., “The Static Testing of a Lockheed P-3 Orion Wing Leading Edge Centre Section,” Aeronautical and Maritime Research Lab. Rept. DSTO-TR-0423, Melbourne, Australia, Nov. 1996.

[6] Bertin, J. J., and Smith, M. L., *Aerodynamics for Engineers*, 2nd ed., Prentice–Hall, Englewood Cliffs, NJ, 1989, Chap. 7.

[7] LabVIEW, Software Package, Ver. 8.0, National Instruments Corp., Austin, TX, 2006.

[8] ABAQUS, Software Package, Ver. 6.4, Hibbitt, Karlsson and Sorensen, Inc., Providence, RI, 2003.